

# PCCP

Accepted Manuscript



This is an *Accepted Manuscript*, which has been through the Royal Society of Chemistry peer review process and has been accepted for publication.

*Accepted Manuscripts* are published online shortly after acceptance, before technical editing, formatting and proof reading. Using this free service, authors can make their results available to the community, in citable form, before we publish the edited article. We will replace this *Accepted Manuscript* with the edited and formatted *Advance Article* as soon as it is available.

You can find more information about *Accepted Manuscripts* in the [Information for Authors](#).

Please note that technical editing may introduce minor changes to the text and/or graphics, which may alter content. The journal's standard [Terms & Conditions](#) and the [Ethical guidelines](#) still apply. In no event shall the Royal Society of Chemistry be held responsible for any errors or omissions in this *Accepted Manuscript* or any consequences arising from the use of any information it contains.

## Limits and Potentials of Quantum Chemical Methods in Modelling Photosynthetic Antennae

Cite this: DOI:  
10.1039/x0xx00000x

www.rsc.org/

Sandro Jurinovich,<sup>a</sup> Lucas Viani,<sup>a,b</sup> Carles Curutchet,<sup>c</sup> and Benedetta Mennucci<sup>a,\*</sup>

Advances in electronic spectroscopies with femtosecond time resolution have provided new information on the excitonic processes taking place during the energy conversion in natural photosynthetic antennae. This has promoted the development of new theoretical protocols aiming at accurately describing the properties and mechanisms of exciton formation and relaxation. In this perspective, we provide an overview of the quantum chemical based approaches, trying to underline both the potentials of the methods and their weaknesses. In particular three main aspects will be analysed, the quantum mechanical description of excitonic parameters (site energies and couplings), the incorporation of environment effects on these parameters through hybrid quantum/classical approaches, and the modelling of the dynamical coupling among such parameters and the vibrations of the pigment-protein complex..

### Introduction

In photosynthesis, light harvesting (LH) takes place in specialised multichromophoric systems called pigment-protein complexes (PPC),<sup>1</sup> where the absorbed energy is converted into excitonic energy which is later on transferred to the reaction centre (RC) complexes to activate the primary charge separation. While RC complexes are very similar among different photosynthetic systems, there is a wide variety of PPC antennae. They differ in the arrangements of chromophores, the chromophore types (e.g. (bacterio)chlorophylls, bilins and carotenoids) and their absorption spectra ranging from the blue to the near-infrared wavelengths. Nevertheless, all PPCs are able to convert light into excitations with very high quantum efficiency. Excitation energy transfer (EET) in PPCs, has traditionally been assumed to happen in the so-called Förster weak-coupling regime.<sup>2</sup> According to this assumption, any electronic coherence between chromophores is rapidly destroyed by stochastic energy fluctuations due to the environment and, as a result, electronic excitations incoherently 'hop' between states localized on individual chromophores. These energy fluctuations are driven by intramolecular vibrations of the chromophores, as well as by the interaction between electronic excitations of the chromophores and vibrational degrees of freedom of the environment.

In the last decades this traditional interpretation of the processes that govern light-harvesting in PPCs has substantially changed thanks to the advances of femtosecond spectroscopy, which has allowed the examination of energy migration processes at the molecular level, revealing that quantum effects

may play a role in the EET dynamics. In particular, starting from the second half of the last decade, the application of the 2-D electronic spectroscopy (2DES) technique to different LH systems has led to a detailed observation of dynamic coherences among exciton states (electronic excited states shared among several electronically-coupled molecules),<sup>3-7</sup> an evidence that EET does not occur in the weak coupling regime. Although it is not unequivocally established that quantum coherence is essential for attaining the highly efficient LH in photosynthesis, it is nowadays well accepted that the coherence effects are involved in the dynamics of ultrafast LH processes.<sup>8-11</sup>

This new scenario has necessarily modified the theoretical analyses, as well as the numerical methodologies used in the simulation of the LH process. In this context, two main strategies have been developed. In the first one, the common approaches used in theoretical physics to simulate quantum transport in open systems are introduced. In these approaches, a model Hamiltonian is used to describe the PPC by generally combining experimental excitonic parameters with a bath of oscillators to include the coupling of the electronic and the environmental modes.<sup>6,12</sup> In the second strategy, instead, electronic structure methods typical of quantum chemistry are used to directly calculate the electronic properties of the pigments, also taking into account the effects of the local environment.<sup>13,14</sup> The two approaches can be considered as complementary, since the first one gives direct access to the quantum-dissipative motion of excitons, while the second one allows the direct calculation of the parameters needed in the first scheme, namely (i) the site energies of the pigments, (ii)

the excitonic coupling between pigments' excitations and (iii) the spectral density of the exciton-vibrational coupling, which describes the dynamical modulation of site energies due to the vibrations of the pigment and its environment. In spite of this evident complementarity, the use of quantum chemical calculations in quantum transport theories has typically been limited. One of the reasons for this lack of connection is that the two classes of methods were born in two distinct communities, the theoretical physicists and the quantum chemists, respectively, and chronologically these methods have evolved almost independently. However, it is now quite clear that a convergence of the two approaches is necessary to achieve a complete and accurate picture of the complexity of processes and interactions, which together determine the photosynthetic light harvesting. At the same time, quantum chemical methods have still to improve in order to represent a real alternative to experiments in predicting all the parameters needed in the description of exciton processes and coherences.<sup>15-24</sup>

This perspective presents a critical overview of these quantum chemical approaches, trying to underline both the potentials of the methods and their weaknesses. The presentation is divided in three main parts, namely the quantum-mechanical (QM) methods developed so far to calculate site energies and exciton couplings, the integration of these methods with models to represent the effects of the environment, and the extension of these multiscale approaches to describe the coupling between electronic and vibrational degrees of freedom.

### QM simulation of site energies and electronic couplings

The most straightforward approach to describe electronic excitations in molecular systems is to explicitly calculate the wave function of the involved electronic states, either using *ab-initio* or semiempirical formulations. Many methods have been proposed so far along this line. In configuration interaction (CI)-type calculations, the electronic wave function is constructed as a linear combination of the ground-state and "excited" determinants, which are obtained by replacing occupied orbitals with virtual ones. To make CI calculations computationally feasible, one can introduce a truncation of the CI expansion such as in the CI-Single (CIS) formalism and/or introduce a semiempirical approach (such as in the ZINDO approach developed by Zerner and coworkers).<sup>25</sup> Both CIS and its semiempirical ZINDO version have been largely applied to describe excitations of LH chromophores obtaining relatively good results;<sup>16,26-28</sup> however such good performances can be due to some unpredictable cancellation of errors and a systematic improvement is difficult to introduce.

Alternatively to the CI truncation, an active space of occupied and virtual orbitals in which all possible "excited" determinants are constructed can be introduced. In this case, a reoptimization of the molecular orbitals is generally used to increase the flexibility of the wave function reduced by the truncation. The

resulting complete active space self-consistent field (CASSCF) approach has been largely used to simulate photochemical processes in the biological context<sup>29,30</sup> while applications to LH systems are not common.<sup>31</sup> One of the reasons is that LH chromophores generally present an extended conjugation and this introduces an evident limitation to CASSCF, which should include a too large number of electrons. In the last years wave function based formulations have been supplemented and in many cases superseded by the linear response (LR) time-dependent DFT approach (TDDFT). The basic idea is to apply time-dependent perturbation theory to first order: before the time-dependent electric field is applied, the molecular system is assumed to be in its electronic ground state determined by solving the corresponding Kohn–Sham equation. When a time-dependent oscillating electric field is applied, the Kohn–Sham orbitals and the corresponding operator, as well as the electronic density, will change. By assuming a linear response, the TDDFT equation for the excitation energies and transition vectors are obtained. The reasons for the enormous success of TDDFT are simple: it in fact combines a great computational efficiency with an extreme ease of use. These two characteristics are extremely important in the case of LH systems as the chromophores are large and most of the wave function based approaches are not applicable due to their excessive computational cost.

Of course TDDFT is not a "perfect method"; in fact while it performs usually very well for valence excited states, it presents severe problems with the correct description of Rydberg and charge-transfer excited states. In the case of excited charge-transfer (CT) states, the excitation energies are much too low (by up to 1 eV) and the potential energy curves do not exhibit the correct 1/R asymptote, where R corresponds to a distance coordinate between the positive and negative charges of the CT state.<sup>32</sup> Presently, several different pathways have been proposed to address the substantial failure of TDDFT for CT states and to correct for it. A very effective way to improve the TDDFT performances for these difficult cases is to split the Coulomb operator of the Hamiltonian into two parts, a short-range and a long-range part, which are treated primarily using a local functional and an exact orbital exchange, respectively. This strategy has led to long-range separated functionals, which have shown to give accurate descriptions of excitation processes in different LH pigments.

TD-DFT presents also another problem due to the single determinant ansatz of DFT; as a result excited states characterized by a significant double excitation character cannot be properly described. To overcome this limit that prevents, for example, the use of TD-DFT methods to investigate excitations of carotenoids, a combination of DFT and a multireference configuration interaction ansatz has been proposed. The resulting DFT/MRCI method<sup>33,34</sup> has shown to be very effective in describing excited states energies and properties of large conjugated systems.<sup>34-37</sup>

The same QM methods used to calculate excitations can also be applied to simulate the couplings among them. In most cases, electronic couplings in LH systems correspond to interactions

between “bright” singlet excitations. This means that the coupling is dominated by Coulomb interactions between transition densities, namely:<sup>38,39</sup>

$$V_{ij}^C = \int d\mathbf{r} \int d\mathbf{r}' \rho_i^{T*}(\mathbf{r}') \frac{1}{|\mathbf{r}' - \mathbf{r}|} \rho_j^T(\mathbf{r}) \quad (1)$$

where  $i$  and  $j$  identify two different excitations. The integral in eq.(1) can be calculated by using the integration algorithm used for DFT. This method can also be further extended to include exchange and correlation effects among transition densities through the expression:

$$V_{ij}^{xc} = \int d\mathbf{r} \int d\mathbf{r}' \rho_i^{T*}(\mathbf{r}') g_{xc} \rho_j^T(\mathbf{r}) \quad (2)$$

where  $g_{xc}$  is the exchange correlation kernel used in the selected DFT formulation while for a HF/CIS description such term reduces to the exact exchange integral.

As a matter of fact, in most applications the transition density is not directly used and an approximated form in terms of transition dipoles or transition atomic charges is instead adopted. As a result, the electronic coupling reduces to a simple dipole-dipole interaction energy or an electrostatic interaction among point charges. The dipole-dipole approximation is the formulation most widely used, given that the values of the transition dipoles can in principle be extracted from absorption and emission spectra of the chromophores. The main limit is that the dipole approximation works well only for inter-chromophoric distances much larger than the dimensions of the chromophores. The transition charge approach instead has been shown to be of larger applicability, although its results strongly depend on the procedure used to get the charges. In most cases a fitting of the electrostatic potential generated by the transition density is applied exactly as it is commonly done for obtaining atomic charges in molecular mechanics force fields: this approach is known as TrEsp (transition charge from electrostatic potential) method.<sup>40</sup> Within such a framework, the Coulomb coupling reduces to:

$$V_{ij}^{TrEsp} = \sum_{K,L} \frac{q_K(i)q_L(j)}{|R_K - R_L|} \quad (3)$$

where  $K$  and  $L$  run on the atoms involved in the excitation  $i$  and  $j$ , respectively, and  $R_X$  are the corresponding spatial positions.

An alternative approach, known as Transition Density Cube (TDC),<sup>41</sup> reformulates the integral in eq.(1) by expressing the transition density as an array of finite-sized volume elements (the transition cube)

$$M_i(r) = V_\delta \int_z^{z+\delta z} \int_y^{y+\delta y} \int_x^{x+\delta x} \rho_i^T(r) dx dy dz \quad (4)$$

where  $\delta_a$  defines the grid size of the density cube, and  $V_\delta$  is the element volume ( $V_\delta = \delta x \delta y \delta z$ ) needed as a practical means of converting charge density per unit volume into charge density per element. Finally, the Coulomb interactions between all the elements of each cube are summed to get the final coupling:

$$V_{ij}^{TDC} = \sum_{k,l} \frac{M_i(k)M_j(l)}{|r_k - r_l|} \quad (5)$$

A completely different strategy to get access to electronic couplings is the one based on the subsystem formulation of density functional theory known as frozen-density embedding (FDE) method.<sup>42</sup> FDE allows to describe a particular subsystem in a Kohn-Sham-type fashion, while the influence of all other subsystems is taken into account in an effective, but entirely quantum chemical way. When the FDE approach is applied to calculations of excitation energies of a system composed of several molecules, a two-step procedure is introduced.<sup>43</sup> First, the uncoupled FDE excitation energies are calculated; i.e., local excitations of all constituent molecules are obtained, embedded in an environment formed by all the other molecules. Local excited states are then obtained for all the subsystems with the approximate form of the FDE generalization to excited states, which restricts the response to the active subsystem only. In a second step, delocalized excited states of the entire aggregate are calculated by coupling these local excitations.

All the methods cited so far should in principle be extended well beyond the single chromophores so to include the effects of the natural environment of antenna PPCs:<sup>13</sup> such an environment always comprises the protein matrix and the solvent (water) but in many cases also a lipid bilayer representing the thylakoid membrane should be explicitly accounted for. Recent studies have attempted to include part of this complex environment using accurate QM descriptions based on FDE<sup>44</sup> and linear-scaling DFT methods.<sup>45</sup> The high computational cost associated to this approaches, however, precludes the possibility to investigate how structural fluctuations modulate site energies or couplings, and in this case multiscale strategies need to be introduced. These strategies are presented and commented in the following section.

## Modelling environment effects

A successful strategy to extend quantum chemistry beyond the isolated molecule is to use a hybrid (or multiscale) approach, in which the QM description is limited to a minimal subsystem (from now on indicated as the “solute”) while the remainder of the system (the “environment”) is treated classically.

A possible strategy along this line is to use a continuum dielectric to model the classical system. Nowadays continuum solvation models have become one of the most used computational techniques in the computational chemistry community. This success arises from their ability to account for the environment effects in a QM calculation at almost the same cost of an analogous calculation for the system in gas phase. This is possible by resorting to a classical continuum description of the environment in terms of its macroscopic dielectric properties. In particular, in modern continuum

solvation models the solute is placed in a proper molecular-shaped cavity inside the dielectric medium representing the environment, and the polarization response of the dielectric medium to the solute charge distribution is obtained by solving the Poisson equation of classical electrostatics. Different flavors of continuum solvation models resort to different strategies to solve this electrostatic problem. Among them, one of the most popular in quantum chemistry, is that adopting a set of induced charges spreading on the cavity surface: the method often called Polarizable Continuum Model (PCM)<sup>46</sup> is actually a family of different methods such as IEFPCM,<sup>47</sup> COSMO<sup>48</sup> (or CPCM<sup>49</sup>) and SS(V)PE<sup>50</sup> just to quote the most popular ones in quantum chemistry.

In all these methods the induced (also called “apparent”) charges, which represent the polarization response of the environment, act to polarize back the QM solute through what is traditionally known as the reaction field. As a result, the solute Hamiltonian becomes an effective Hamiltonian defined as:

$$H_{eff} = H_0 + \sum_k q_k(\epsilon) V_k^{QM} \quad (6)$$

where the first term is the Hamiltonian of the isolated solute and the second term is the electrostatic interaction between the solute and the apparent charges  $q_k$  ( $V_k^{QM}$  is the electrostatic potential operator originated from the QM solute and calculated at the cavity surface). The charges  $q_k$  are determined by the QM electrostatic potential calculated on the cavity surface; as a result, the operator in eq.(6) will depend on the QM charge distribution and the solution of the effective Schrödinger equation will automatically lead to mutually polarized QM and classical subsystems. The same mutual polarization can be kept during the excitation process of the QM solute; in that case, however, a further specificity of the environment response has to be introduced. The differences in the characteristic response times of the various degrees of freedom of the environment may lead to a “solvation” regime in which the slow components (i.e., those arising from translations and rotations of the environment molecules) are no longer equilibrated with the solute upon excitation. The resulting “nonequilibrium” regime will possibly relax into a new equilibrium in which the environment is allowed to relax all its degrees of freedom including the slow ones. Especially for highly polar environments, “equilibrium” and “nonequilibrium” regimes represent very different configurations and their energy difference is generally known as “reorganisation energy”. The “nonequilibrium” solvation can be properly described within the continuum framework introducing a separation of the surface charges into a fast (or dynamic) contribution, mimicking the polarization of the electronic charge of the environment molecules, and a slow (or inertial) contribution, due to the nuclear and molecular motions. The fast (or dynamic) charges are obtained by using the same expression used for the full equilibrium case but this time the environment response is represented by the optical component ( $\epsilon_\infty$ ) of the dielectric permittivity and the solute electrostatic potential

refers to the new solute charge distribution (namely to the excited state in a vertical excitation process). By contrast, the slow component is obtained as the difference of the full polarization and the fast component both calculated in equilibrium with the initial charge distribution of the solute. This nonequilibrium approach has been successfully applied to the simulation of site energies in PPCs defining an effective dielectric function for the heterogeneous environment (e.g. protein+solvent). Generally, values between 4 and 15 are used for the static  $\epsilon$  while a value of 2 is used for the optical component: the large variability in the static value is generally explained to account for the presence of the water, which mixing with the protein makes the environment more polar.

While continuum models represent an efficient and robust approach to describe “average” electrostatic and polarization effects of the environment, they present an evident limitation in properly accounting for specific interactions between the “solute” and its close environment as well as for important heterogeneities in the environment response. Both these two aspects can become very important in simulating electronic processes in LH pigments for which the environment comprises the protein matrix, eventually the membrane, and the solvent, and the local effects can largely change from one pigment to the other. A very effective way to account for these heterogeneities is to replace the continuum description with a molecular mechanics (MM) force field. The resulting QM/MM approaches<sup>51-56</sup> are very well known in computational chemistry and biology and recently they have become quite popular also for the modeling of LH systems.

There is variety of force fields (FF) that have been parameterized to describe biological systems. Most of them use fixed charges to represent the electrostatic interactions but, more recently, important efforts have been devoted to include polarization effects.<sup>57</sup> Different polarizable models have been developed, either using fluctuating charges,<sup>58-62</sup> Drude oscillators<sup>63,64</sup> or induced dipoles.<sup>65-67</sup> When these FF are coupled to a QM description, a similar effective Hamiltonian to that described for continuum models is introduced,<sup>68-73</sup> namely if we use a polarizable FF based on induced dipoles we get:

$$H_{eff} = H_0 + \sum_i q_i V_i^{QM} - \frac{1}{2} \sum_i \mu_i \cdot E_i^{QM} \quad (7)$$

where the induced dipoles are determined assigning a (generally) isotropic point polarizability (in addition to the charge  $q_i$ ) to each atom ( $i$ ) of the environment and  $E_i^{QM}$  is the electrostatic field on the same atom due to the QM solute. Now the mutual polarization effects are obtained due to the induced dipoles, which are determined by the total electric field acting on the corresponding atoms due to MM sites and the QM solute.

Also QM/MM methods have been largely applied to describe excitation processes.<sup>56</sup> If a non-polarizable FF is used, (i.e. if a standard electrostatic embedding is applied) only the inertial part of the environment response is taken into account: during the excitation process, in fact, the “electrostatic” embedding is

kept frozen. To properly include the fast part of polarization, instead, a polarizable embedding is necessary: for example the induced dipoles in eq.(7) can account for the electronic rearrangement of the environment upon excitation. Polarizable QM/MM methods have been applied to the simulation of site energies in different PPCs and the obtained results generally show a different behavior with respect to the standard QM/MM with electrostatic embedding.<sup>28,74,75</sup> If these differences correspond to a better description of the environment effects for the LH processes in PPCs is still difficult to say as a direct comparison to experiments is not possible. However, what appears clearly is that for solutes in standard solvents the use of a polarizable MM environment gives an accurate description of solvation effects by successfully accounting for both short and long-range interactions.<sup>56</sup> In fact, when strong specific solute-solvent interactions are not present, the resulting picture coincides with the one obtained with continuum models, while when the solute can strongly and specifically interact with the solvent molecules of the first solvation shells important differences are found, leading to a better agreement with the experiments. One delicate aspect of polarizable FFs is the correct parameterization. For example, when induced dipoles are used the parameterization cannot be limited to the atomic polarizabilities but also the fixed charges need to be recalculated so to be coherent with the induced dipoles. These parameterizations are nowadays available for proteins and other biological macromolecules but in many cases the cofactors present in the PPC need to be parameterized ad-hoc.

Besides site energies, explicit account of polarization is a key feature in the modeling of environment effects in electronic couplings. In this case, the heterogeneous environment of pigments embedded in PPCs can significantly modulate pigment-pigment interactions and substantial deviations arise if such an effect is described using either atomistic or continuum dielectric approaches.<sup>26</sup>

More in details, the presence of an environment can lead to strong differences in the coupling due to two main effects. The first one is exactly the same leading to changes in the site energies: namely the environment can change both the geometrical and the electronic structure of the pigments thus modifying their transition properties, i.e. site energies, transition dipoles and transition densities. These changes will be automatically reflected in different couplings. Secondly, if the environment can polarize, the direct Coulomb interaction between excitations in different pigments will be “screened” by the environment. These screening effects were traditionally taken into account in the dipole-dipole approximation to the coupling in terms of an effective dielectric constant through a  $1/\epsilon_{\text{eff}}$  scaling term, an approximation already present in the early formulation of Förster theory. The same scaling factor has also been adopted in TrEsp and TDC approaches. In more refined continuum formulations that take into account the shape of the molecule inside the dielectric medium, the screening can be self-consistently obtained by calculating the transition densities in the presence of the proper perturbation (see eq. 6) and adding an explicit “environment” term to the Coulomb

coupling.<sup>76</sup> By using the PCM framework such term can be written as<sup>39</sup>

$$V_{ij}^{PCM} = \sum_k q_k^{PCM}(\rho_j^T) \int d\mathbf{r}' \rho_i^{T*}(\mathbf{r}') \frac{1}{|\mathbf{r}' - \mathbf{r}_k|} \quad (8)$$

where  $q_k^{PCM}$  are the charges induced on the cavity surface by the electronic transition in the chromophore  $j$ . These charges, which are determined assuming a nonequilibrium response, allow to describe a screening that depends not only on the electronic transitions involved but also on the inter-pigment distance and orientation.<sup>77</sup> Indeed, application of this strategy to a large series of pigment pairs from LH complexes revealed a strong exponential attenuation of screening effects at distances below 20 Å, a common situation in LH antennae.<sup>77</sup>

A similar strategy can be applied to a polarizable QM/MM formulation; in that case the “screening” term need to be reformulated as:<sup>69</sup>

$$V_{ij}^{MMPol} = - \sum_l \boldsymbol{\mu}_l(\rho_j^T) \cdot \int d\mathbf{r}' \frac{(\mathbf{r}' - \mathbf{r}_l)}{|\mathbf{r}' - \mathbf{r}_l|^3} \rho_i^{T*}(\mathbf{r}') \quad (9)$$

where now the induced dipoles act to screen the interaction between the two transition densities.

The two polarizable formulations have been shown to give very similar results on average, while they can lead to quite different effects when single pairs of pigments are analyzed.<sup>26</sup> Due to differences in the polarizability of the local environment around each pigment in fact the  $V^{MMPol}$  term can change significantly and the resulting net coupling varies from one pair to another.

All QM/MM methods (including or not polarization effects) need to be coupled with a proper sample of different configurations of the environment. The application of these methods to a single structure (for example the crystallographic structure) can in fact lead to large errors due to the presence of artificially strong pigment-residue interactions coming both from resolution limits and from the fact that temperature induced relaxation effects are not included. A correct application of QM/MM methods should instead include molecular dynamics (MD) simulations of the PPC in its natural environment at the correct temperature; from these simulations, many different configurations can be generated and used for the calculation of the site energies and couplings. In Fig. 1 we quantify the difference that can be obtained from the two approaches, namely a “static” one based on a single (crystal) structure and a “dynamic” one using averages on different configurations obtained from MD. In the plots we report the site energies calculated for the 8 bilins of phycoeritrin 545 (PE545), a PPC present in cryptophyte algae, and the 8 bacteriochlorophylls of Fenna-Matthews-Olson (FMO), a PPC present in green sulfur bacteria, as obtained by using a polarizable QM/MM approach.

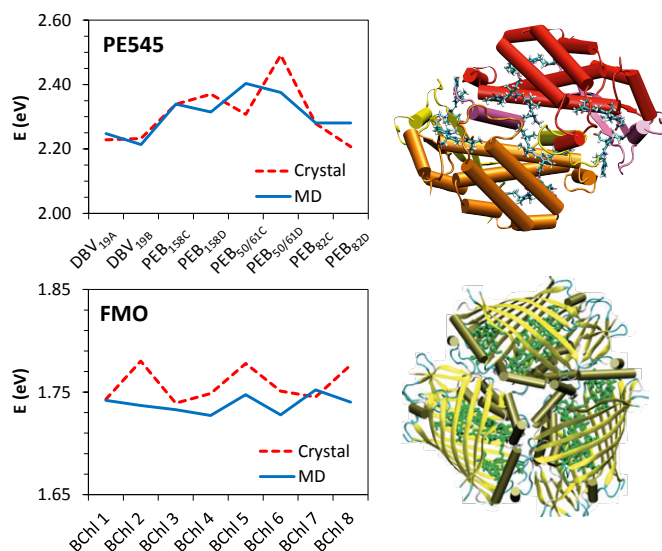


Figure 1: QM/MMPol calculations of site energies (in  $\text{cm}^{-1}$ ) for PE545 and FMO obtained either using the crystal structure or averaging over many different configurations extracted from an MD simulation. The results are taken from Ref. [74] for PE545 and Ref. [75] for FMO.

As it can be seen from Fig.1 the sampling among different configurations not only can change the relative order of the site energies but it generally “smooths out” the differences among similar pigments, as it is the case of the PEB<sub>50/61C</sub> and PEB<sub>50/61D</sub> bilins in the PE545 complex, which are located in an almost symmetric environment. This has shown to be very important to correctly reproduce the experimental optical spectra.<sup>74,75</sup>

The large dimensions of PPCs presently prevent a QM simulation of their dynamics but instead MD based on classical force fields are used: such a decoupled strategy where the electronic description is treated at quantum chemical level while the “dynamic” one is treated with classical force fields can introduce problems as we’ll discuss in the following section.

## The coupling between excitations and vibrations

Beyond the modulation of the average excitonic parameters (site energies and electronic couplings) exerted by the environment, it is also important to describe the dynamical modulation of such parameters due to the coupling among the pigments and the nuclear degrees of freedom of the system. This coupling leads to stochastic fluctuations in the energy levels of the pigments that determine spectral line shapes and drive incoherent transfers and exciton localization.

The spectral density,  $J(\omega)$ , describes the information about the coupling among excitons and matrix vibrations. In quantitative models of EET in photosynthetic antennae,  $J(\omega)$  is typically modeled as a sum of two terms:

$$J(\omega) = J_0(\omega) + J_{\text{vib}}(\omega) \quad (10)$$

where  $J_0(\omega)$  describes the coupling of electronic transitions to a continuum of low-frequency damping modes due to the protein and solvent surrounding the pigments, whereas  $J_{\text{vib}}(\omega)$  describes the coupling to high-frequency modes, mostly intramolecular in nature. Several expressions are often used to describe  $J_0(\omega)$ ,<sup>78</sup> whereas  $J_{\text{vib}}(\omega)$  is usually modelled as a collection of harmonic oscillators.

Experimentally, both  $J_0(\omega)$  and  $J_{\text{vib}}(\omega)$  can be measured by using site-selective spectroscopies, such as spectral hole-burning and fluorescence line-narrowing techniques.<sup>79</sup> These techniques, however, provide spectral densities for the lowest exciton state, or an average over several thermally populated low energy states. The complexity of measuring  $J(\omega)$  for the individual pigments in a PPC explains why most simulations of LH dynamics in PPCs assume the same spectral density for all pigments.<sup>8,74</sup> The coupling to vibrations with energies that commensurate the energy difference between exciton states has been suggested to play a key role in understanding quantum coherent oscillations observed in PPCs.<sup>11,80,81</sup> The structured nature of  $J(\omega)$  can vary for different pigments in a PPC, specially in the low-energy range characterized by interactions with the local environment. Indeed, experiments show that the shape of  $J(\omega)$  varies among different PPCs.<sup>82-84</sup> Thus, the assumption of a common spectral density for all pigments can obscure the impact of individual features in quantum coherence. On the other hand, it is difficult to assess experimentally whether the pigments are coupled to independent or common modes in the environment. In the first case, a coupling to common protein vibrations could lead to correlated fluctuations in the energies of the electronic states: this was first postulated as the origin of the long-lived coherences experimentally observed.<sup>3</sup>

An attractive way to overcome the limits in experimental techniques consists in the theoretical estimation of  $J_{\text{vib}}(\omega)$ , and several groups have contributed with important advances in this direction.<sup>15,17-24,85-89</sup> The most common approach used so far consists on the estimation of  $J(\omega)$  by simulating the time-evolution of the site energies, combining ground-state classical MD simulations with QM/MM calculations of the excited states along the trajectory. Within this strategy, the spectral density is obtained from the Fourier transform of the autocorrelation function of site energy fluctuations:<sup>16,85,89</sup>

$$J(\omega) = \frac{\beta\omega}{\pi} \int_0^\infty C^{cl}(t) \cos(\omega t) dt \quad (11)$$

where  $\beta = 1/(k_B T)$  and  $C^{cl}(t)$  is the classical autocorrelation function of the fluctuation of the site energies. Because  $J(\omega)$  is obtained from a classical correlation function, Eq. (11) includes a classical prefactor to negate the temperature dependence of the classical correlation function, as clarified by Valleau and co-workers.<sup>89</sup>

This MD-QM/MM scheme allows the simultaneous determination of both  $J_0(\omega)$  and  $J_{\text{vib}}(\omega)$  contributions to the spectral density, and the coupling among environmental and intramolecular modes is fully taken into account. However, the

large computational cost associated to this strategy, involving massive QM/MM excited-state calculations along the MD trajectories, typically for each 2-5 fs in order to capture the fastest oscillations in site energies, poses some problems. An important limitation is the classical treatment of the nuclei in the MD, which has been suggested as the cause for the severe overestimation of the coupling to high-frequency intramolecular modes of the pigments in  $J_{\text{vib}}(\omega)$ . Whereas this problem can be solved by resorting to MD simulations performed at the QM level, the cost of such simulations precludes at present their practical use in the study of PPCs. Another problem associated to the accurate determination of  $J_{\text{vib}}(\omega)$  is the quality of the geometries used in the QM/MM calculations of the excitation energies, given that the MD simulation is performed along a potential energy surface described by an approximate classical force field. This problem is expected to introduce considerable errors in excited state calculations, which should optimally be performed on geometries obtained from accurate QM methods. A possible solution is the derivation of specialized force fields being able to describe with accuracy the vibrational modes and fluctuations of each pigment. On the other hand, the limited MD times that can be simulated make low-frequency protein motions difficult to resolve, reducing the quality of the spectral density described by  $J_0(\omega)$  at such frequencies.

In order to overcome the limitations of the MD-QM/MM strategy outlined above, some groups have proposed alternative strategies in which  $J_0(\omega)$  and  $J_{\text{vib}}(\omega)$  are obtained separately. Renger and co-workers have proposed a strategy where  $J_0(\omega)$  is obtained from a classical normal mode analysis (NMA) of the protein modes by assessing the coupling of electronic transitions along each mode coordinates, while keeping the intramolecular pigment modes frozen.<sup>21</sup> Spectral densities in good qualitative agreement with experiments have been obtained using this approach. An important advantage of this strategy over MD-based approaches is the possibility to determine the impact of very low-frequency motions in  $J_0(\omega)$  and in the presence of eventual electronic correlations. A potential drawback, however, is its inability to account for the multiple minima that characterize protein energy landscapes, especially in flexible backbones, given that the NMA analysis is performed for a single minimum. A similar strategy has been proposed by Jing and co-workers to estimate  $J_{\text{vib}}(\omega)$  from NMA analysis of the ground and excited state potential energy surfaces of the chromophores using quantum chemical methods.<sup>18</sup> The advantage of this strategy relies on the description of the pigment modes at a quantum mechanical level, so the geometry mismatch problem encountered in MD-based strategies over classical trajectories is overcome. This approach has been shown to give vibrational frequencies and Huang-Rhys factors in reasonable agreement with experiments. Although the strategies mentioned above overcome some of the important limitations of MD-based approaches through separate calculation of the  $J_0(\omega)$  and  $J_{\text{vib}}(\omega)$  contributions to the spectral density, an important limitation is the neglect of the coupling among the pigment and the protein/solvent modes, which has

been recently shown to significantly modulate the distribution of intramolecular modes in the bilin pigments of PE545,<sup>24</sup> as it will be discussed in the following subsections.

### The impact of the environment in spatial and electronic correlations

Theoretical studies have suggested that the existence of correlation between the fluctuations of the constituents of the excitonic matrix may assist the formation and modulation of coherent states among the chromophores in PPCs via the tuning of the intermolecular transfer rates and population oscillations.<sup>90,91</sup> The investigation of these possible correlations through MD-QM/MM approaches can be divided in two parts. First, spatial correlations between the positions of the atoms of different pigments can be quantified by analyzing the configurations obtained along the MD trajectory. Afterwards QM/MM calculations of excitonic parameters can be performed on the same MD configurations to see if the spatial correlations are reflected in the excitonic matrix, i.e. if they induce any correlation among site energies and/or couplings.

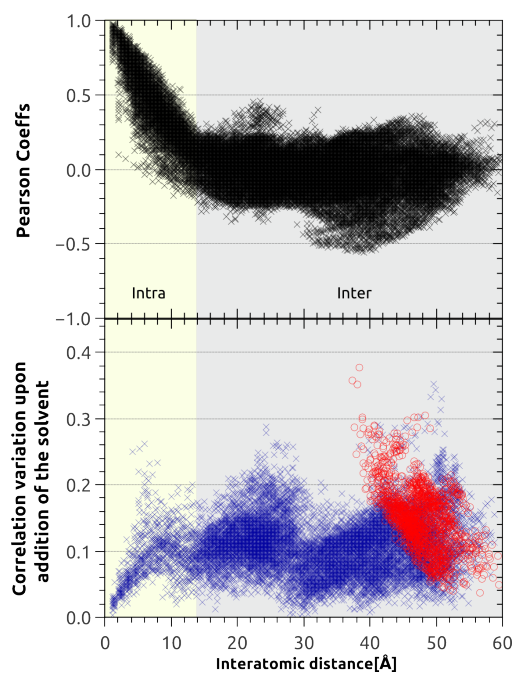


Figure 2: Spatial correlations (in terms of the Pearson coefficient) between the positional fluctuations of all atom pairs of the eight bilins in PE545 (top), variation of the same coefficients for the atoms of the pigment DBV<sub>19A</sub>, upon addition of the solvent (bottom). The correlations with respect to the atoms of the other DBV<sub>19B</sub> pigment are highlighted in red (bottom). The background colors indicate the range with predominant intra and intermolecular correlations.

An interesting finding resulting from the spatial analysis is the important role played by the solvent. In particular, the presence of spatial correlations can be strongly connected to how the pigments are exposed to the solvent. For PPCs in which the pigments are spatially “screened” from the solvent by the protein matrix, negligible intermolecular spatial correlations are observed, such as the case of the FMO.<sup>87</sup> On the contrary, in

PPCs where the pigments directly interact with the solvent molecules, higher spatial correlations are observed. An example of the latter case is the PE545, where high spatial correlation is observed up to an intermolecular distance of 40 Å,<sup>28</sup> see Figure 2-top. Such high correlation at long distances was mainly attributed to a solvent-induced effect by comparing two different MD simulations of PE545, one in water and one in gas phase. An example of the differences between the two simulations is shown in Figure 2-bottom. In particular, the highest variations (up to ~0.4 in the correlation) are associated to correlations of the atoms of the two DBV bilins (highlighted in red), which have an average intermolecular distance of 45 Å and are the pigments more exposed to the solvent.

Despite the presence or not of significant spatial correlations, correlations between site energy fluctuations were found to be negligible for various PPCs. However, coupling/coupling correlations were found to be significant (of the order of 0.4-0.6 for both PE545 and FMO). It is important to note that although the impact of coupling/coupling correlations in the EET dynamics is expected to be lower than energy correlations, their real role has still to be quantified.<sup>90</sup> In the case of cross-correlations, e.g. site energies/couplings correlations, differences between different PPCs have been observed. For example, in FMO, such correlations were not observed when the couplings were computed in the TrEsp framework, although larger values were predicted within the point-dipole formalism. In PE545, such correlations always feature large values when both site energy and coupling are related to the same pigment, regardless the method used to compute the couplings. An explanation for the larger cross-correlations in PE545 may lie on the nature of the pigments. In this complex, in fact, the bilins are flexible linear tetrapyrrole molecules where any distortion in the geometry, such as torsion angles in the conjugated backbone, would directly modify the site energy, transition densities, and the orientation of the transition dipoles, thus simultaneously impacting the site energies and the couplings. In FMO, instead, the planar and more rigid chlorophylls are less susceptible to large geometrical deformations and changes in the relative orientation of the transition dipoles. The cross-correlations in PE545 were found to be predominantly negative, suggesting that an increase/decrease on the site energy value is followed, in average, by a decrease/increase of the absolute value of its coupling to the other pigments. Such anticorrelations may have significant consequences on both the coherences and the transfer rates.<sup>90,92,93</sup>

### The impact of the environment in pigment vibrations and spectral densities

Beyond the modulation of site energies and electronic couplings, the environment plays a key role in determining the spectral density  $J(\omega)$ . The geometrical “flexibility” of the pigments embedded in the protein matrix may change substantially when compared to the free pigment in solution. Thus, both the frequencies and the exciton-vibrational

couplings for intramolecular modes can be strongly modulated by the local protein environment. The impact of such modulation is here illustrated for the PE545 complex.<sup>24</sup> Figure 3-top reports the distribution of the vibrational modes of the PEB<sub>82c</sub> bilin computed using a normal mode (NMA) analysis of the free pigment and a quasi-harmonic (QH) analysis of the pigment embedded in the protein matrix, respectively.

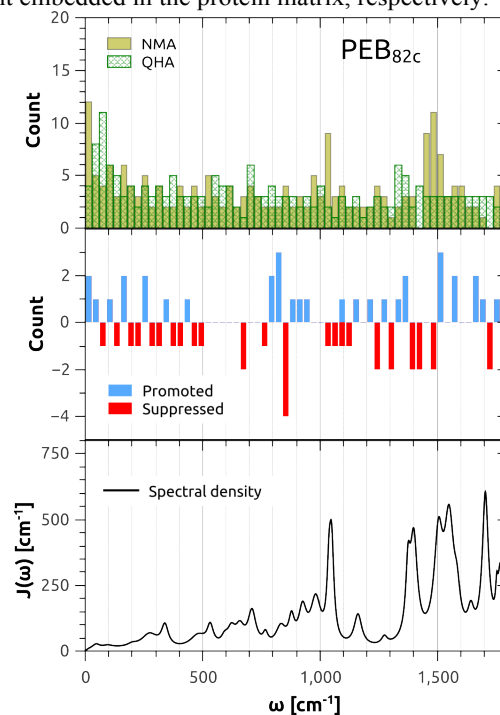


Figure 3: Distribution of normal modes and quasi-harmonic modes of the pigment PEB<sub>82c</sub>, (top), variations in the quasi-harmonic analysis distribution between the solvated and gas-phase MD simulation (middle), and calculated spectral density (bottom) of the bilin in the PPC.

The NMA analysis probes the vibrations around a single minimum, while the QH analysis aims at characterizing the global extent of the configurational space accessible to the system during an MD simulation. The comparison between the NMA and QH modes allows assessing the impact of the protein and solvent environment in the intrinsic vibrations of the pigments. Such comparison indicates that the accumulation of modes around 1000 and 1500 cm<sup>-1</sup> observed for the isolated pigment is smoothed out when coupled to the protein modes. The solvent also plays a role in redistributing the vibrational frequencies, thus accumulating or reducing the number of modes in some frequency regions. This is shown in Figure 3-middle for the same PEB<sub>82c</sub> bilin. This analysis is done by comparing the QH analysis distribution of vibrational frequencies obtained from two different MD simulations of PE545, one in water and one in gas phase: blue/red bars indicate a region with higher/lower accumulation of modes when the PPC is solvated. It is interesting to note that such modulation caused by the spatial interactions with the solvent directly affects the spectral density of the pigment, see Figure 3-bottom, since the strongest modifications occur in the

frequency regions where stronger exciton-phonon couplings are found.

## Conclusions

In this perspective we have presented a critical overview of current quantum chemical methodologies used to model photosynthetic antennae. The accurate determination of site energies, electronic couplings and spectral densities, which constitute the main ingredients needed for a quantitative description of the light harvesting process, still constitutes a considerable challenge for the theoretical and computational chemistry. The correct estimation of the site energy ladder within a given PPC is a key aspect, for example, in order to understand the features of its optical spectra as well as the EET dynamics and spatial directionality. Because site energy differences are small, typically in the order of 50-1000 cm<sup>-1</sup>, small differences in the computational approach adopted often lead to significantly different pictures, a problem evident in the large variety of results obtained so far by different groups for the FMO complex.<sup>27,31,44,45,75,94,95</sup> Progress in this direction is expected to occur around three basic points: (i) the adoption of more accurate QM methods beyond semiempirical or TD-DFT approaches; (ii) improvements in the multiscale models aimed at describing the impact of the environment in excited-state properties beyond the electrostatic approximation; (iii) elimination (or alleviation) of the problem related to the mismatch arising from the use of geometries obtained from classical MD simulations in QM excited-state calculations. This latter point, in our opinion, is the key one as it is clear that not only it can affect the quality of the excitonic parameters averaged along the trajectory but it represents a critical issue in the estimation of their fluctuations and therefore in the simulation of spectral densities. Indeed, the difficulty to accurately describe the impact of intramolecular and environmental modes – characterized by a multitude of timescales – on the excited states of the pigments, makes accurate predictions of spectral densities one of the most challenging issues in the field. Important advances in the three outlined aspects are therefore necessary to allow quantum chemistry to really become the state-of-the-art approach in the field; in the upcoming years we expect that these advances will follow two alternative directions, one aiming at developing more and more accurate force fields for the pigments and the other allowing explicit QM/MM (eventually including polarization effects) molecular dynamics.

## Acknowledgements

The European Research Council (ERC) through the Starting Grant proposal n. 277755 (EnLight) is acknowledged by S.J., L.V., and B.M.. L.V. also acknowledges the Universidad Carlos III de Madrid, the European Commission (7th Framework Programme - grant n° 600371), el Ministerio de Economía y Competitividad of Spain (COFUND2013-40258) and Banco Santander. C.C. acknowledges support from the Ministerio de Economía y Competitividad (MINECO) of Spain (grants CTQ2012-36195 and RYC2011-

08918) and the Agència de Gestió d'Ajuts Universitaris i de Recerca from the Generalitat de Catalunya (GENCAT) (SGR2014-1189).

## Notes and references

<sup>a</sup> Dipartimento di Chimica e Chimica Industriale, University of Pisa, via G. Moruzzi 3, 56124 Pisa, Italy. Email: Benedetta.mennucci@unipi.it

<sup>b</sup> Institute for Fluid Dynamics, Nanoscience and Industrial Mathematics, Universidad Carlos III de Madrid, Av. de la Universidad 30, E-28911 Leganés, Spain.

<sup>c</sup> Departament de Físicoquímica, Facultat de Farmàcia, Universitat de Barcelona, Av. Joan XXIII s/n, 08028 Barcelona, Spain.

1. R. E. Blankenship, *Molecular Mechanisms of Photosynthesis*, John Wiley & Sons, 2014.
2. T. Forster, *10TH SPIERS MEMORIAL LECTURE*, 1959, 1–11.
3. H. Lee, Y.-C. Cheng, and G. R. Fleming, *Science*, 2007, **316**, 1462–1465.
4. G. S. Engel, T. R. Calhoun, E. L. Read, T.-K. Ahn, T. Mančal, Y.-C. Cheng, R. E. Blankenship, and G. R. Fleming, *Nature*, 2007, **446**, 782–786.
5. E. Collini, C. Y. Wong, K. E. Wilk, P. M. G. Curmi, P. Brumer, and G. D. Scholes, *Nature*, 2010, **463**, 644–647.
6. A. Ishizaki and G. R. Fleming, *Annu. Rev. Condens. Matter Phys.*, 2012, **3**, 333–361.
7. C. Y. Wong, R. M. Alvey, D. B. Turner, K. E. Wilk, D. A. Bryant, P. M. G. Curmi, R. J. Silbey, and G. D. Scholes, *Nature Chemistry*, 2012, **4**, 396–404.
8. A. Kollí, E. J. O'Reilly, G. D. Scholes, and A. Olaya-Castro, *J Chem Phys*, 2012, **137**, 174109.
9. M. del Rey, A. W. Chin, M. B. Plenio, and S. Huelga, *J Phys Chem Lett*, 2013, **4**, 903–907.
10. E. Collini, *Chem. Soc. Rev.*, 2013, **42**, 4932–4947.
11. E. J. O'Reilly and A. Olaya-Castro, *Nat Commun*, 2014, **5**, 3012.
12. V. I. Novoderezhkin and R. Van Grondelle, *Phys Chem Chem Phys*, 2010, **12**, 7352–7365.
13. B. Mennucci and C. Curutchet, *Phys Chem Chem Phys*, 2011, **13**, 11538–11550.
14. C. König and J. Neugebauer, *Chemphyschem*, 2011, **13**, 386–425.
15. C. Olbrich and U. Kleinekathoefer, *J Phys Chem B*, 2010, **114**, 12427–12437.
16. C. Olbrich, J. Struempfer, K. Schulten, and U. Kleinekathoefer, *J Phys Chem Lett*, 2011, **2**, 1771–1776.
17. M. Aghtar, J. Strumpfer, C. Olbrich, K. Schulten, and U. Kleinekathoefer, *J Phys Chem Lett*, 2014, **5**, 3131–3137.
18. Y. Jing, R. Zheng, H.-X. Li, and Q. Shi, *J Phys Chem B*, 2011, **116**, 1164–1171.
19. S. Shim, P. Rebentrost, S. Valleau, and A. Aspuru-Guzik, *Biophysj*, 2012, **102**, 649–660.
20. T. Fujita, J. Huh, S. K. Saikin, J. C. Brookes, and A. Aspuru-Guzik, *Photosynth Res*, 2014, **120**, 273–289.
21. T. Renger, A. Klinger, F. Steinecker, M. Schmidt am Busch, J. Numata, and F. Müh, *J Phys Chem B*, 2012, **116**, 14565–14580.
22. H. W. Kim, A. Kelly, J. W. Park, and Y. M. Rhee, *J Am Chem Soc*, 2012, **134**, 11640–11651.
23. E. Rivera, D. Montemayor, M. Masia, and D. F. Coker, *J Phys Chem B*, 2013, **117**, 5510–5521.
24. L. Viani, M. Corbella, C. Curutchet, E. J. O'Reilly, A. Olaya-Castro, and B. Mennucci, *Phys Chem Chem Phys*, 2014, **16**, 16302.
25. 1973, **32**, 111–134.
26. C. Curutchet, J. Kongsted, A. Munoz-Losa, H. Hossein-Nejad, G. D. Scholes, and B. Mennucci, *J Am Chem Soc*, 2011, **133**, 3078–3084.
27. J. Gao, W.-J. Shi, J. Ye, X. Wang, H. Hirao, and Y. Zhao, *J Phys Chem B*, 2013, **117**, 3488–3495.
28. L. Viani, C. Curutchet, and B. Mennucci, *J Phys Chem Lett*, 2013, **4**, 372–377.
29. S. Gozem, F. Melaccio, H. L. Luk, S. Rinaldi, and M. Olivucci, *Chem. Soc. Rev.*, 2014, **43**, 4019–18.
30. I. Rivalta, A. Nenov, G. Cerullo, S. Mukamel, and M. Garavelli, *Int*

- J Quantum Chem*, 2013, **114**, 85–93.
31. N. H. List, C. Curutchet, S. Knecht, B. Mennucci, and J. Kongsted, *J Chem Theory Comput*, 2013, **9**, 4928–4938.
32. A. Dreuw and M. Head-Gordon, *Chem Rev*, 2005, **105**, 4009–4037.
33. S. Grimme and M. Waletzke, *J Chem Phys*, 1999, **111**, 5645–5655.
34. C. M. Marian and N. Gilka, *J Chem Theory Comput*, 2008, **4**, 1501–1515.
35. J. P. Gotze and W. Thiel, *Chem Phys*, 2013, **419**, 247–255.
36. O. Andreussi, S. Knecht, C. M. Marian, J. Kongsted, and B. Mennucci, *J Chem Theory Comput*, 2015, **11**, 655–666.
37. S. Knecht, C. M. Marian, J. Kongsted, and B. Mennucci, *J Phys Chem B*, 2013, **117**, 13808–13815.
38. C. Hsu, G. Fleming, M. Head-Gordon, and T. Head-Gordon, *J Chem Phys*, 2001, **114**, 3065–3072.
39. M. Iozzi, B. Mennucci, J. Tomasi, and R. Cammi, *J Chem Phys*, 2004, **120**, 7029–7040.
40. M. E. Madjet, A. Abdurahman, and T. Renger, *J Phys Chem B*, 2006, **110**, 17268–17281.
41. B. Krueger, G. Scholes, and G. Fleming, *J Phys Chem B*, 1998, **102**, 5378–5386.
42. 1993, **97**, 8050–8053.
43. J. Neugebauer, *J Chem Phys*, 2007, **126**, 134116–134112.
44. C. König and J. Neugebauer, *J Chem Theory Comput*, 2013, **9**, 1808–1820.
45. D. J. Cole, A. W. Chin, N. D. M. Hine, P. D. Haynes, and M. C. Payne, *J Phys Chem Lett*, 2013, **4**, 4206–4212.
46. J. Tomasi, B. Mennucci, and R. Cammi, *Chem Rev*, 2005, **105**, 2999–3093.
47. E. Cancès, B. Mennucci, and J. Tomasi, *J Chem Phys*, 1997, **107**, 3032–3041.
48. A. Klamt, *Wiley Interdisciplinary Reviews: Computational Molecular Science*, 2011, **1**, 699–709.
49. V. Barone and M. Cossi, *J Phys Chem A*, 1998, **102**, 1995–2001.
50. D. Chipman, *J Chem Phys*, 2000, **112**, 5558–5565.
51. J. Gao, *Accounts Chem Res*, 1996, **29**, 298–305.
52. R. A. Friesner and V. Guallar, *Annu Rev Phys Chem*, 2005, **56**, 389–427.
53. T. Vreven and K. Morokuma, *Annual Reports in Computational Chemistry*, 2006, **2**, 35–51.
54. H. Lin and D. G. Truhlar, *Theor Chem Acc*, 2007, **117**, 185–199.
55. H. M. Senn and W. Thiel, *Angew Chem Int Edit*, 2009, **48**, 1198–1229.
56. B. Mennucci, *Phys Chem Chem Phys*, 2013, **15**, 6583.
57. A. Warshel, M. Kato, and A. V. Pislakov, *J Chem Theory Comput*, 2007, **3**, 2034–2045.
58. A. RAPPE and W. Goddard, *J Phys Chem-US*, 1991, **95**, 3358–3363.
59. R. A. Bryce, R. Buesnel, I. H. Hillier, and N. A. Burton, *Chem Phys Lett*, 1997, **279**, 367–371.
60. R. Chelli and P. Procacci, *J Chem Phys*, 2002, **117**, 9175–9189.
61. S. Patel, A. Mackerell, and C. Brooks, *J Comput Chem*, 2004, **25**, 1504–1514.
62. D.-X. Zhao, C. Liu, F.-F. Wang, C.-Y. Yu, L.-D. Gong, S.-B. Liu, and Z.-Z. Yang, *J Chem Theory Comput*, 2010, **6**, 795–804.
63. G. Lamoureux, A. Mackerell, and B. Roux, *J Chem Phys*, 2003, **119**, 5185–5197.
64. P. E. M. Lopes, J. Huang, J. Shim, Y. Luo, H. Li, B. Roux, and A. D. MacKerell Jr., *J Chem Theory Comput*, 2013, **9**, 131105131241005.
65. J. W. Ponder, C. Wu, P. Ren, V. S. Pande, J. D. Chodera, M. J. Schnieders, I. Haque, D. L. Mobley, D. S. Lambrecht, R. A. DiStasio Jr., M. Head-Gordon, G. N. I. Clark, M. E. Johnson, and T. Head-Gordon, *J Phys Chem B*, 2010, **114**, 2549–2564.
66. J. Wang, P. Cieplak, J. Li, J. Wang, Q. Cai, M. Hsieh, H. Lei, R. Luo, and Y. Duan, *J Phys Chem B*, 2011, **115**, 3100–3111.
67. J. Wang, P. Cieplak, J. Li, T. Hou, R. Luo, and Y. Duan, *J Phys Chem B*, 2011, **115**, 3091–3099.
68. M. A. Thompson and G. K. Schenter, *J. Phys. Chem.*, 1995, **99**, 6374–6386.
69. C. Curutchet, A. Munoz-Losa, S. Monti, J. Kongsted, G. D. Scholes, and B. Mennucci, *J Chem Theory Comput*, 2009, **5**, 1838–1848.
70. F. Lipparini and V. Barone, *J Chem Theory Comput*, 2011, **7**, 3711–3724.
71. J. Olsen and J. Kongsted, *Adv Quantum Chem*, 2011, **61**, 107–143.
72. E. Boulanger and W. Thiel, *J Chem Theory Comput*, 2012, **8**, 4527–4538.
73. S. Caprasecca, S. Jurinovich, L. Viani, C. Curutchet, and B. Mennucci, *J Chem Theory Comput*, 2014, **10**, 1588–1598.
74. C. Curutchet, V. I. Novoderezhkin, J. Kongsted, A. Munoz-Losa, R. Van Grondelle, G. D. Scholes, and B. Mennucci, *J Phys Chem B*, 2013, **117**, 4263–4273.
75. S. Jurinovich, C. Curutchet, and B. Mennucci, *Chemphyschem*, 2014, **15**, 3194–3204.
76. C. Hsu, S. Hirata, and M. Head-Gordon, *J Phys Chem A*, 2001, **105**, 451–458.
77. G. D. Scholes, C. Curutchet, B. Mennucci, R. Cammi, and J. Tomasi, *J Phys Chem B*, 2007, **111**, 6978–6982.
78. A. Kell, X. Feng, M. Reppert, and R. Jankowiak, *J Phys Chem B*, 2013, **117**, 7317–7323.
79. R. Jankowiak, M. Reppert, V. Zazubovich, J. Pieper, and T. Reinot, *Chem Rev*, 2011, **111**, 4546–4598.
80. V. Tiwari, W. K. Peters, and D. M. Jonas, *Proceedings of the National Academy of Sciences*, 2013, **110**, 1203–1208.
81. A. W. Chin, J. Prior, R. Rosenbach, F. Caycedo-Soler, S. F. Huelga, and M. B. Plenio, *Nature Physics*, 2013, **9**, 113–118.
82. M. Rätsep and A. Freiberg, *J Lumin*, 2007, **127**, 251–259.
83. M. Rätsep, J. Pieper, K.-D. Irrgang, and A. Freiberg, *J Phys Chem B*, 2008, **112**, 110–118.
84. J. Pieper, M. Rätsep, I. Trostmann, H. Paulsen, G. Renger, and A. Freiberg, *J Phys Chem B*, 2011, **115**, 4042–4052.
85. A. Damjanovic, I. Kosztin, U. Kleinekathöfer, and K. Schulten, *Phys Rev E*, 2002, **65**, 031919.
86. L. Janosi, I. Kosztin, and A. Damjanovic, *J Chem Phys*, 2006, **125**.
87. C. Olbrich, J. Strumpfer, K. Schulten, and U. Kleinekathöfer, *J Phys Chem B*, 2011, **115**, 758–764.
88. M. Aghtar, J. Strumpfer, C. Olbrich, K. Schulten, and U. Kleinekathöfer, *J Phys Chem B*, 2013, **117**, 7157–7163.
89. S. Valteau, A. Eisfeld, and A. Aspuru-Guzik, *J Chem Phys*, 2012, **137**, 224103.
90. S. M. Vlamming and R. J. Silbey, *J Chem Phys*, 2012, **136**, 055102.
91. P. Huo and D. F. Coker, *J Chem Phys*, 2012, **136**, 115102.
92. X. Chen and R. J. Silbey, *J Chem Phys*, 2010, **132**, 204503–204513.
93. J. Wu, F. Liu, Y. Shen, J. Cao, and R. J. Silbey, *New J Phys*, 2010, **12**, 105012–18.
94. M. S. A. Busch, F. Müh, M. E.-A. Madjet, and T. Renger, *J Phys Chem Lett*, 2011, **2**, 93–98.
95. C. Olbrich, T. L. C. Jansen, J. Liebers, M. Aghtar, J. Struempfer, K. Schulten, J. Knoester, and U. Kleinekathöfer, *J Phys Chem B*, 2011, **115**, 8609–8621.